An apparatus for rapid and nondestructive comparison of masks and respirators

Cite as: Rev. Sci. Instrum. **91**, 114101 (2020); https://doi.org/10.1063/5.0015983 Submitted: 31 May 2020 . Accepted: 29 September 2020 . Published Online: 19 November 2020

Donal Sheets, Jamie Shaw, Michael Baldwin, David Daggett, Ibrahim Elali, DErin B. Curry, DIlya Sochnikov, and Jason N. Hancock







ARTICLES YOU MAY BE INTERESTED IN

Compact integrated optical sensors and electromagnetic actuators for vibration isolation systems in the gravitational-wave detector KAGRA

Review of Scientific Instruments 91, 115001 (2020); https://doi.org/10.1063/5.0022242

Review of Scientific Instruments New Products

Review of Scientific Instruments 91, 119501 (2020); https://doi.org/10.1063/5.0035170

Geometrical effects of microchannel plates: Grazing incidence operation of time-of-flight mass spectrometry and comparison to standard carbon foil

Review of Scientific Instruments 91, 113107 (2020); https://doi.org/10.1063/5.0021482



Your Qubits. Measured.

Meet the next generation of quantum analyzers

- Readout for up to 64 gubits
- Operation at up to 8.5 GHz, mixer-calibration-free
- Signal optimization with minimal latency





An apparatus for rapid and nondestructive comparison of masks and respirators

Cite as: Rev. Sci. Instrum. 91, 114101 (2020); doi: 10.1063/5.0015983 Submitted: 31 May 2020 • Accepted: 29 September 2020 •







Published Online: 19 November 2020

Donal Sheets,^{1,2,a)} Damie Shaw,² Michael Baldwin,³ David Daggett,⁴ Ibrahim Elali,⁵ Erin B. Curry,^{1,2} Ilya Sochnikov,^{1,2} and Jason N. Hancock^{1,2}

AFFILIATIONS

- Institute of Material Science, University of Connecticut, Storrs, Connecticut 06269, USA
- ²Department of Physics, University of Connecticut, Storrs, Connecticut 06269, USA
- Department of Diagnostic Imaging, University of Connecticut Health Center, Farmington, Connecticut 06030, USA
- Department of Molecular and Cell Biology, University of Connecticut, Storrs, Connecticut 06269, USA
- ⁵Division of Nephrology, University of Connecticut Health Center, Farmington, Connecticut 06030, USA

ABSTRACT

The SARS-CoV-2 global pandemic has produced widespread shortages of certified air-filtering personal protection equipment and an acute need for rapid evaluation of breathability and filtration efficiency of proposed alternative solutions. Here, we describe experimental efforts to nondestructively quantify three vital characteristics of mask approaches: breathability, material filtration effectiveness, and sensitivity to fit. We focus on protection against aqueous aerosols >0.3 μ m using off-the-shelf particle, flow, and pressure sensors, permitting rapid comparative evaluation of these three properties. We present and discuss both the pressure drop and the particle penetration as a function of flow to permit comparison of relative protection for a set of proposed filter and mask designs. The design considerations of the testing apparatus can be reproduced by university laboratories and medical facilities and used for rapid local quality control of respirator masks that are of uncertified origin, monitoring the long-term effects of various disinfection schemes and evaluating improvised products not designed or marketed for filtration.

Published under license by AIP Publishing. https://doi.org/10.1063/5.0015983

I. INTRODUCTION

SARS-CoV-2 is an infectious virus that can be transmitted via respiratory aerosols. ¹⁻⁶ Face masks capable of blocking virus-containing aerosol particles typically use state-of-the-art textile technologies, such as corona-charged melt-blown polypropylene. This material is capable of supporting electrostatic filtration and is used in the production of the high-filtration efficiency, breathable, tightly fitting, inexpensive, and normally accessible respirators certified as N95. Dwindling supplies of personal protective equipment (PPE) in clinics and hospitals ⁹⁻¹² combined with the need for the general population to wear masks ¹³ has strained supply chains and led to local efforts to produce new technologies, as well as many proposed do-it-yourself mask approaches, in an effort to meet these needs. ^{14,15} Shortages have led to numerous responses such as the increased production of certified and uncertified respirators, the use of

backstock mask and respirator stockpiles, attempts to disinfect and reuse existing PPE, and localized efforts by universities, medical professionals, and the public to produce new technologies and improvised designs. ^{16–18} In this environment, many claims of efficacy are made, while the data supporting such claims are often incomplete or lacking. Effective evaluation and adoption of PPE remains a critical aspect of best practice in medical care and public health for controlling the spread of SARS-CoV-2. ^{19–25,60–64}

The urgent need for rapid methods to assess the efficacies of these supplies and designs as compared to existing, certified products has motivated strong academic and public interest in respiratory protection devices and evaluation to control the spread of SARS-CoV-2.^{17,26–32} This document describes an experimental apparatus devised and developed at the University of Connecticut and in collaboration with clinicians from the University of Connecticut Health Center during a rapid response period in March and April

a) Author to whom correspondence should be addressed: donal.sheets@uconn.edu

2020. This apparatus is capable of making comparisons of essentially any existing or proposed mask design or candidate filter material with respect to filtration of aqueous aerosol particles in the <1.0 μm diameter range. While not designed as a certification device, the relative performance data generated by the apparatus allow informed decisions regarding respiratory protection and quantitative assessment of the relative roles of filtration, breathability, and fit. The materials tester component could also be used for building and hospital filtration media testing where infection may be circulated with inadequate filters in hospitals, schools, long-term care facilities, and indoor public spaces. Beyond the urgent needs during pandemic, this apparatus can be used for building air filter quality control, quality control of dust personal protective equipment (PPE) on large construction sites or large-scale abatement projects, and research of new high-performance filtration materials.

II. EXPERIMENTAL APPARATUS

A. Overview

Our approach relies on a simulated environment that represents a potential clinical, employment, educational, or other shared air space condition, 19 illustrated in Fig. 1. Conceptually, an aerosol containing presumably virus-laden particles is exhaled by an infected person (IP) into a shared air space (SA), where it is potentially inhaled into the respiratory system of a susceptible person (SP). Each of these terms corresponds to a separate chamber in our apparatus (Fig. 1). Briefly, the apparatus (Fig. 2) consists of a fiberglass glove box (Labconco 50 350, Kansas City, MO, USA) with a sealable load-lock chamber mounted on a large swinging door that can be closed and sealed quickly using toggle clamps. The large chamber of the glove box represents the SA. A gas pump, a needle valve, and a flow meter control and measure the flow from a controlled aerosolized air source through the SA and into the load-lock chamber representing the SP, after passing through either a mask-donning mannequin head (Laerdal Airway Management Trainer, Stavanger,

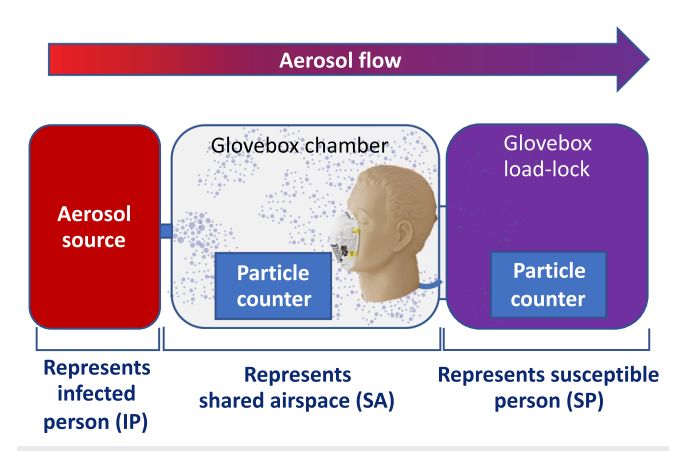


FIG. 1. Schematic representation of the experimental apparatus. An aerosol source chamber represents the infected person (IP), a glove box main chamber represents the shared air space (SA), and the glove box load lock represents the susceptible person (SP). Controlled aerosolized air flows through the system from left to right, and pressures and particulates are measured for comparison studies at fixed environmental conditions.

Norway) or a clamp-style materials tester based on Kwik-Flange (KF) vacuum fittings, depending on the state of two ball valves [Fig. 2(c)]. Identical sets of particle meters and calibrated sensors in the SA and SP chambers monitor the size-dependent aerosol particle distribution, humidity, temperature, and pressure on each side of the mask or material. The two modalities of the apparatus permit assessment of (a) a mask on a mannequin head with realistic respiratory geometry or (b) material-only properties regarding breathability and filtration efficiency over selected sections of a mask. Each of these modalities provides vital information to assess the practicality and effectiveness of protection against potentially infectious aerosols. As controls, mask and material experiments include measurements with an open system, as well as a high-performance mask (e.g., 3M-1860 N95) for comparison. Below, we detail different components of the system following the air flow, from IP to SA to SP chambers.

B. Aerosol source

SARS-CoV-2 virions range in size from 60 nm to 140 nm³³ and can be transmitted via droplets containing multiple copies of the virus generated from respiratory fluids during breathing, talking, and coughing. A respiratory droplet 0.1 nl in volume has a radius of 2.8 μ m and a mass of 100 ng and can contain as much as 1 ng salt and 1 ng protein; however, the dominant component is water. ³⁴ Following expulsion into the environment, water evaporates rapidly, and the fluid constituency influences the ultimate size of the suspended droplet nuclei ^{35–37} that may carry infectious virions. ³⁸ Infectious SARS-CoV-2 is believed to be transmitted by both relatively large respiratory droplets (>5 μ m in diameter) and finer aerosols containing microdroplets and droplet nuclei (<5 μ m). ^{4,39–41}

Aqueous aerosol sources used in regulatory tests of filter media exploit similar physics to those of pathogen transmission by effectively producing a fine mist of water with known solute concentration and controlled evaporation in an experimental setup. A variety of challenge aerosol sources are used in regulatory tests. For example, NIOSH 42 CFR 84 requires neutralized NaCl particles with a mean diameter of 0.075 \pm 0.02 μm at a concentration of <200 mg/m³, while the FDA-PFE uses unneutralized latex spheres 0.1 μm in diameter. With component substitutions, each of these test regimes could be achieved based upon our chamber.

For the measurements presented in this work, we simulate infected respiratory aerosols with a chamber in which an ultrasonic nebulizer element submersed in tap water produces Faraday surface waves and cavitation, ⁴² emitting a plume of aqueous aerosol. The use of an aqueous aerosol based on tap water is advantageous for the continuous, rapid assessment of mask and material filtration. For the tests presented here, we have measured the tap water conductivity to be equivalent to that of an ~0.013% NaCl solution. While tap water produces ample particle concentration (~10 μ g/m³) in the size range appropriate for mask studies (0.3 μ m-1.0 μ m; Fig. 3), it does not significantly load mask materials and does not contaminate the system components as readily as higher concentration aqueous salt aerosols, such as the 2% NaCl solution typically used in the NIOSH certification protocol. ^{43,44}

There are many possible methods to produce aqueous aerosols, such as Laskin nozzles, ultrasonic atomizers, piezoelectric nebulizers, and vibrating orifice aerosol generators^{45,46} that can produce

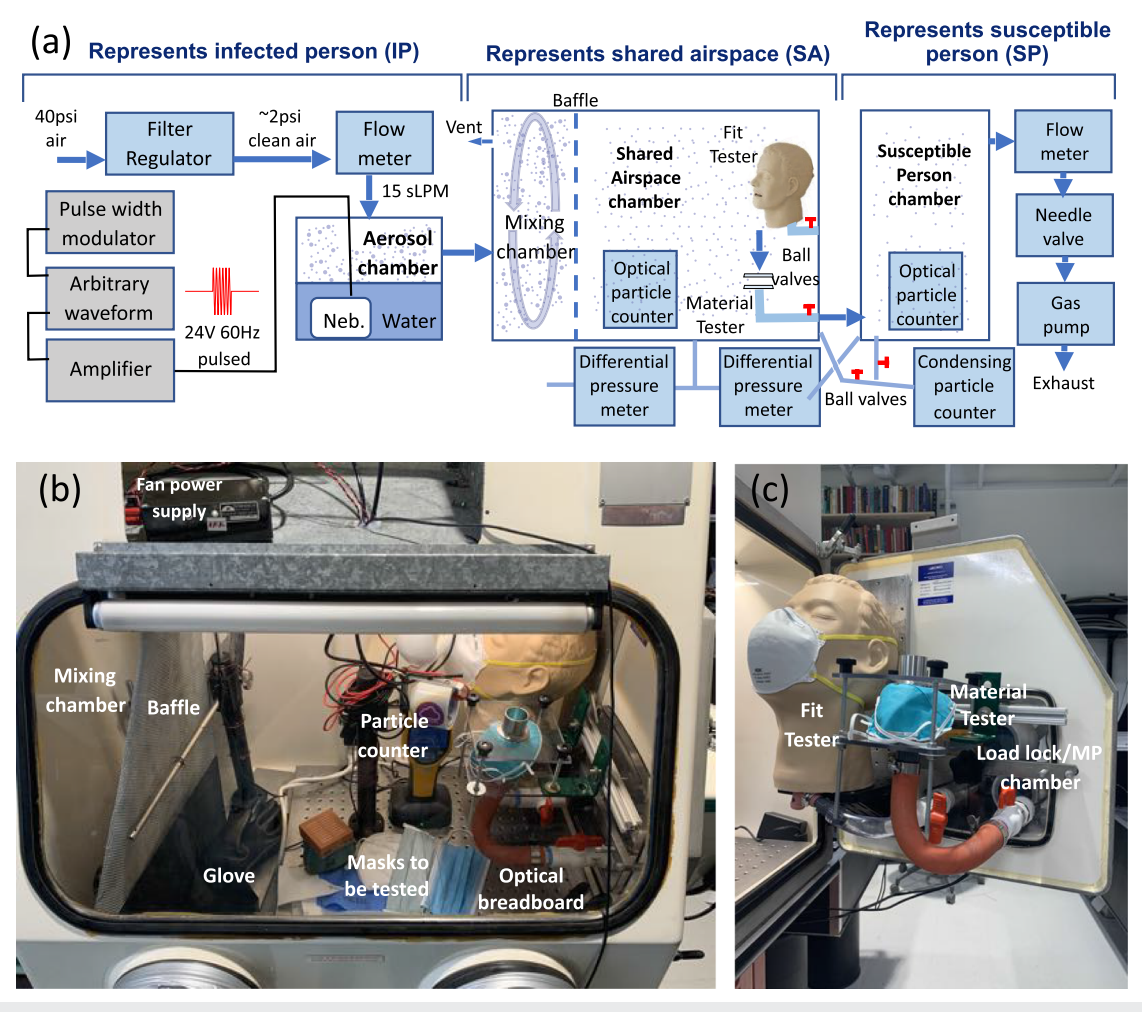


FIG. 2. (a) Schematic experimental setup with materials tester active. Clean air is filtered and aerosolized by flowing over the surface of water containing a piezoelectric nebulizer (Neb.) element powered by 24VAC sine pulses arriving at 0.2 Hz and variable duty cycle. The aerosolized air flows into a mixing chamber and through baffles, where it is drawn through a mask-donning mannequin head (disabled in the figure) or a materials clamp tester and into the SP chamber. Optical and condensing particle meters measure humidity, pressure, temperature, and count particulate matter 0.02 μ m-10 μ m in diameter. [(b) and (c)] Photographs of the apparatus testing two N95 reference masks

very high concentrations of particles; the aerosol-generating subsystem used in the experiments presented here is outlined in Fig. 2(a), left side. The nebulizer consists of an immersed piezoelectric element that is driven by a 60 Hz 24 V amplitude sine-wave modulated at 0.2 Hz with a variable duty cycle, producing an unneutralized plume of fine mist into the air flow stream once every 5 s. The duration of the plume is controlled by varying the duty cycle of the input square wave, permitting fine control of the aerosol content of the air flowing through the system, and is realized independently of the flow dynamics such as pressure drop and air currents.

We find that after the mixing stage, there is no observable time structure in the aerosol content and the distribution is unaffected by the duty cycle of >1%. The measured relative humidity level in our main chamber is determined by ambient conditions and rarely exceeds 40% relative humidity. We have identified three reliable methods to achieve controlled 24 V 60 Hz pulse duration.

Using benchtop electronics available in a research laboratory, we used an arbitrary waveform generator (AWG; Instek 2000 series, Taiwan) amplified with a waveform amplifier (Accel TS250, USA) to increase the current supplied to drive the element. If the nebulizer is on, we find that 45 s of operation completely saturates the particle counters in the SA (>650 particles/cm³ >0.3 μ m). The AWG is gated with a square wave pulse with a variable duty cycle from a function generator (Instek 2000 series, Taiwan). As a second option, we have gated a 110 V power line directly using a solid-state relay (Jekewin SSR-40DA) operated via a function generator providing square wave input with a variable duty cycle. Finally, a commercial short period repeat cycle timer (BN-LINK, BND-60/U97A) can perform the modulation directly from line voltage with sealed components in a standalone device, although we find that the available modulation frequency limits are limited with this option.

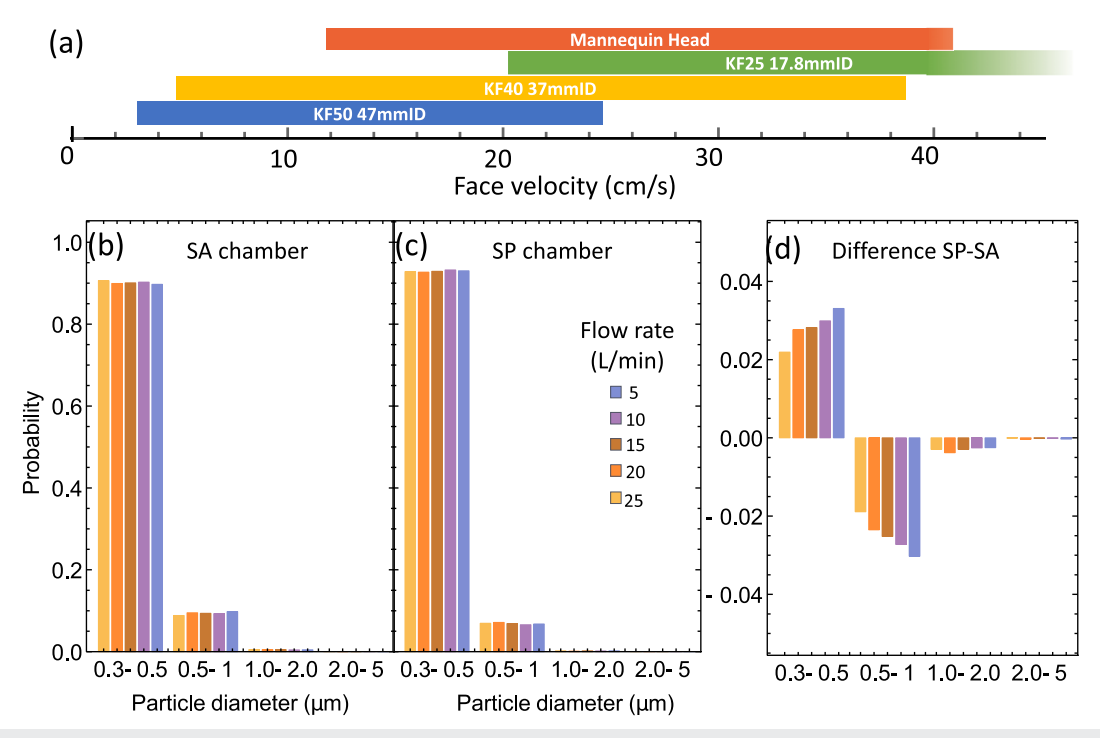


FIG. 3. (a) Available face velocities using the various fitting attachments. The flow range used in this study was 5 l/min–25 l/min, but the variable area permits a wide range of face velocity spanning the most common certification standards in the range of 9 cm/s–25 cm/s. Particle distributions in the (b) SA and (c) SP chambers, normalized by the total number of particles in each. The concentration in the 0.3 μ m–1.0 μ m channel is ~10 μ g/m³. (d) shows the difference SP-SA and highlights a shift in the distribution to smaller particles, consistent with a small degree of evaporation.

Aerosol was sampled in the SA chamber using an optical particle counter (Fluke 985 clean room particle detector, USA) and found to have a particle distribution mostly below 1 μ m, consistent with prior reports on a similar device⁴² after significant evaporation. Aerosol in this size range is both challenging to filter using woven or common fabric materials and also makes up the vast majority of exhaled particles⁴⁷ and so is suitable for our apparatus. In modifications of the present system, a diffusion dryer or cyclone can be introduced between the SP and SA chambers to provide additional control over humidity and particle size.

C. Mixing chamber

Once the aerosol is pushed into the SA glove box chamber, two DC motor fans, arranged to set up a vertical circulating flow pattern on the left end of the glove box chamber, rapidly mix the aerosol and prevent settling. During this mixing process, large droplets evaporate and approach an equilibrium size distribution. Applying the standard theory for settling time and terminal speed under Stokeslaw drag force developed for spherical aerosol particles in air, ⁴⁸ we estimate the settling velocities of the $0.3~\mu m-1~\mu m$ aqueous aerosol observed in our chamber to be in the range 1~cm/h-10~cm/h, which implies that the aerosol in the chamber would stay well mixed over a few hours, more than sufficient to reach the mask and materials testers in the SA chamber. Solutes such as NaCl or KCl can be

added to the water in the IP chamber and control the particle size distribution as well as concentration.

The well-mixed aerosol population crosses through a baffle made from two layers of steel mesh with a 3.5 mm grid pattern. Using a hot wire anemometer, the measured air speed in the mixing chamber is of order 100 cm/s but less than 1 cm/s on the downstream side of the baffles. For a circular flow pattern of the mixing chamber having approximately 1 m circumference, we estimate that the chamber churns the air 5 times per aerosol pulse delivered 5 times/s, consistent with the lack of detectable time structure in the SA chamber.

D. Particle counters

Particle counters are an important component of the apparatus. Common types of particle counters include laser-based optical particle counters (OPCs) and are commonly used to monitor air quality in clean room, hospital, and laboratory environments. OPCs are typically used in standards such as the NIOSH 42 CFR part 84, ASTM 2100, and ASTM 2299. ^{49,50} In our apparatus, aerosolized air was sampled on the right side of the SA chamber using OPCs before transiting the mask or material into the SP chamber where a matching set of counters measured the aerosol distribution for comparison. Three different types of meters are employed to span different aerosol particle size distribution ranges.

Fast readout particle counters developed by PurpleAir (UT, USA) are based upon the PLANTOWER 5001 (Beijing Plantower, China) OPCs. In collaboration with PurpleAir, we have gratefully acquired test software permitting complete readout and logging of the two counters per unit (two units/chamber) at ~1 s intervals. These counters have been studied under various conditions and correlate reasonably well with higher-performing and more costly particle counters. They do not work as well in high humidity environments (>50%), are known to have lowered efficiency (~50%) in the finest particle channel (0.3 μ m-1.0 μ m), and are designed to perform well at high particle concentration levels. These meters are used during experiments to make decisions during data acquisition as well as in analysis.

NIST-traceable Fluke 985 integrating and logging OPCs are placed in each chamber during a typical run. These counters are best suited for lower number concentrations. The devices are programmed to collect over 15 s intervals with 2 min wait times between.

A single TSI P-Trak 8525 ultrafine condensing particle counter is used to detect the integrated particle count in the 0.02 μm –1.0 μm size range. This device consumes reagent grade isopropanol and is placed outside the chamber and connected to a small ball valve manifold with equal-length tubing to the SA and SP chambers.

E. Mask tester

A mannequin head was removed from a Laerdal Airway Management Trainer, an educational product designed to give an accurate representation of human air flow pathways. The lungs were removed, and the right main bronchus was closed with a rubber stopper and hose clamp. The left main bronchus was also hose-clamped onto a $\frac{1}{2}$ in. PVC barb fitting to $\frac{3}{4}$ in. NPT pipe thread, a short segment of vinyl tubing, and another barb into a PVC ball valve that is open when the mask tester is in use. The valve feeds through an acrylic door to the load-lock chamber using PVC pipe fittings and seals with an O-ring.

While the mannequin provides a useful gauge of the leak rate of the mask, it is limited in addressing dynamic factors such as head and jaw movement while talking as well as variation of head forms between individuals. The Center for Disease Control uses mechanized mannequin based tests to emulate rainbow passage fitment tests commonly used in hospital settings. ⁵² Below, we show how a fixed mannequin mask tester can be used to compare fit approaches.

F. Materials tester

To rapidly identify whether the fit or material is the weak link in any proposed mask design, we have enabled an option to disable the mannequin head and open the SA-SP chamber connections though a dedicated materials tester, as detailed in Appendix A. This jig is activated by opening a PVC ball valve connecting the SP chamber through PVC hard line or thick-wall $\frac{3}{4}$ in. rubber tubing terminating in a KF25 vacuum fitting pointing upward and held fixed in the center of a 6×6 in.² polycarbonate plate mounted to the glove box door. $4\frac{1}{4}$ in.-20 threaded rods in each corner of the polycarbonate plate form a materials clamp with a matching plate above and a second KF25 fitting. Importantly, our apparatus permits wide control of the average speed of aerosol impingement on the filter media, known as the face velocity, discussed in Sec. III A. In order to access lower face velocities, discussed below, we can introduce one of two conical adapters (KF25 to KF40 or KF25 to KF50) and matching vacuum fittings (KF40 or KF50, respectively) to distribute the flow over a larger area. Figure 3(a) summarizes the parameters achievable with each of these fittings, and Fig. 4(a) shows the penetration and pressure drops over these choices of fitting. This configurability permits access to face velocities up to 170 cm/s at 25 l/min flow with a 17.8 mm hole in the KF25 fitting and down to the lower value of 2.9 cm/s at 5 l/min flow with a 47 mm hole in the KF50 fitting. Our system could be operated at higher flows with a suitable replacement of the mass flow meter.

We point out that this materials tester has several advantages over common regulatory methods for inserting material into the

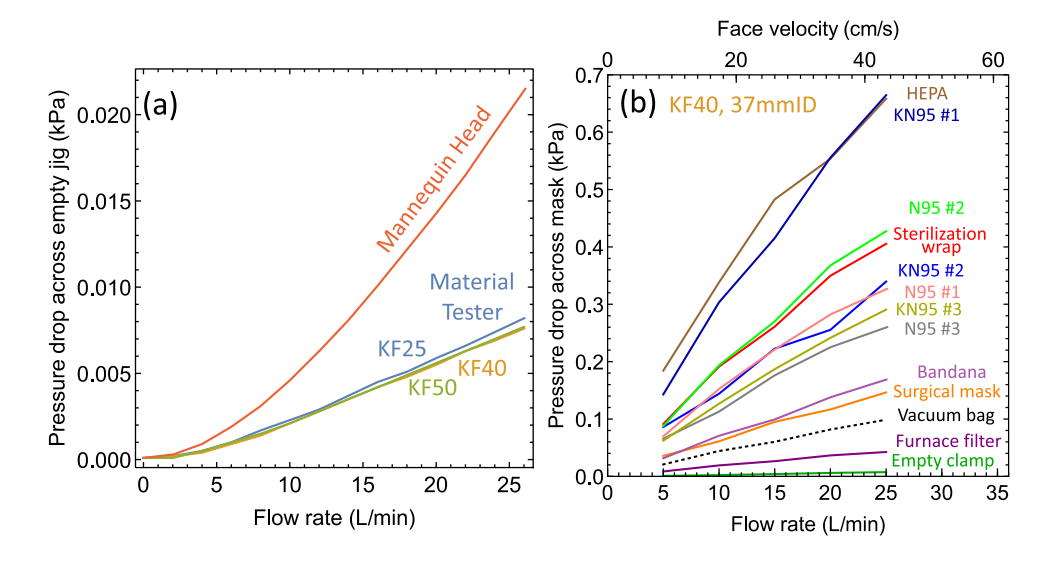


FIG. 4. Breathability measurements. (a) Pressure drop across a mannequin wearing no mask and a materials clamp with various vacuum fittings sizes, demonstrating the sensitivity of the pressure drop measurement. (b) Pressure drop vs flow across some filters, masks, and filter material candidates in the materials tester using the KF40 fitting. A pressure drop spread between quality and mediocre masks is substantial, making some masks dangerous to use if high flow impedance draws contaminants through leaks and gaps.

flow stream. For example, the NIOSH 42 CFR part 84 requires sealing a mask or respirator using beeswax to a metal plate with a hole separating the chambers. This configuration is necessarily destructive and prohibits a given sample from being tested faithfully a second time once the seal is broken.

Both the mask and materials testers were mounted inside the glove box door, as shown in Fig. 2(c), in order to permit short tubes in geometries that do not move when the door is opened. To facilitate this mounting, a small strip of optical breadboard was attached using O-ring-sealed bolts to the inside of the glove box door to present suitable and versatile mounting options. Both the mask and materials tester can be accessed using the box's gloves enabling rapid swapping of the samples without the need to wait for the chambers to equilibrate. The ability to swap out samples consecutively without altering environmental conditions is helpful for direct comparison of material approaches.

G. Particulate distribution

Experiments at various conditions indicate that pure aqueous aerosol <1 μm in diameter evaporates quickly, reaching equilibrium size in less than 1 s.^{33,47} Figures 3(b) and 3(c) show the normalized size distribution of aerosol measured in the SP and SA chambers, showing that for tap water aerosol sources, >90% of the observed particles are in the finest size bin of 0.3 µm— and there is only a weak redistribution of sizes on transit from the SA to SP. Figure 3(d) shows the difference of these plots (SP - SA) and reveals a small but detectable redistribution of the aerosol before and after the mask or materials tester. The shape of the distribution changes no more than 3.3% between bins and does not significantly alter our comparative filtration measurements of masks and materials. Note that the difference depends only slightly upon flow, with a greater change occurring for lower flow as expected from evaporation. We estimate for the slowest flow rates used here (5 l/min), and aerosol is drawn from one chamber to another in less than 3 s.

In addition to changes in the shape of the distribution, there is also a flow-dependent penetration of the total number of aerosol particles >0.3 μ m through an open pipe. This arises from a well-known effect of aerosol collisions in the connecting pipe ⁵³—the longer the aerosol spends in the pipe, the more the chance for a collision with a pipe wall and removal from the flow stream. As expected, we observe the lowest transmission of an empty pipe for the lowest flow rate

We can estimate the total aerosol mass concentration from the measured count distribution under typical operating conditions. For a nebulizer duty cycle of 6% in tap water, we observe ~19 000 counts in the 0.3 μ m–0.5 μ m size bin in a 0.1 L volume of sampled air. Assuming the standard particle density of 1 g/cm³, 48 our mass concentration is in the range of 6.3 μ g/m³ in this size bin. Considering all other size bins under similar considerations, we estimate no more than 15 μ g/m³. Mass concentration considerations are important when studying the effects of particle loading on the filter materials and mask performance. For our measurements at a single flow rate, the filter is active for less than 30 min/mask, accumulating less than 12 μ g at a high 25 l/min flow rate. In contrast, the NIOSH 42 CFR 84 test requirements are performed under heavy loading of up to 200 mg. While we do not explore loading-dependent filtration

performance here, such studies could be extended from our chamber apparatus by using high concentration aqueous aerosol.

To isolate the penetration of the mask or material, it is necessary to address the known loss of particles in the system when there is no mask present. For each measurement, the number of particles N is measured for the SP and SA chambers with a mask in the clamp $(N_{m,SP}, N_{m,SA})$ as well as the same for an open pipe or mannequin head $(N_{o,SP}, N_{o,SA})$. To account for this loss, we divide the observed penetration $N_{m,SP}/N_{m,SA}$ of a given mask/material by a reference measurement of the open jig $N_{o,SP}/N_{o,SA}$ at a given flow, permitting isolation of the penetration P of the mask or material, $P = 100 \times N_{m,SP}N_{o,SA}/N_{m,SA}N_{o,SP}$, and the filtration efficiency is f = 100 - P. We emphasize that our goal is a comparison of mask approaches to one another rather than an absolute certification standard.

H. Flow control

A gas pump (Oxford GF10, UK), a needle valve, and a thermal mass flow meter (TSI 4100, USA) connected to the SP chamber sustain constant and controllable flow of gas through the system. The gas pump is located in a separate pump room, connected by $\frac{1}{4}$ in. tubing to a constrictive needle valve that permits fine control of the flow through the system. A thermal mass flow meter and a protective inlet filter recommended by the manufacturer is installed upstream and reads mass flow with a precision of 0.001 l/min. Feedback mass flow control could be introduced easily although we find that the drift in flow is not a limitation in our measurements.

III. EXPERIMENTAL RESULTS

A. Breathing, pressure drop, flow, and face velocity

Crucial for high-performance masks is that low effort is required to inhale or exhale through a mask or mask material. This breathability property is typically quantified using the pressure drop at a given flow rate, with a smaller pressure drop being more breathable. The flow requirements on breathing are given by the situation, which for humans at rest is around 5 l/min–6 l/min on average assuming a tidal volume of 0.5 l cycled 10 times/min–12 times/min. Time-resolved measurements of human respiration give flow rates in the range of 10 l/min peak exhalation, with larger inhalation flow rates of order 25 l/min. Exertional breathing in healthy humans can reach peak inhalation flow exceeding 600 l/min. The NIOSH tests for N95 certification are performed at 85 l/min, where >95% of the 0.3 μ m NaCl particles are blocked. 8

For any mask, the flow Q is distributed over the active filter material area A with a mask-averaged speed called the face velocity v = Q/A. Some standards for mask testing such as NIOSH specify flow, while others such as FDA specify the face velocity. ^{24,55} For the NIOSH test over a typical half face respirator such as the 3M-1860 of area 150 cm², the mask-averaged face velocity is around 9.3 cm/s, while the same exercise for a surgical mask of area 100 cm² results in a face velocity of 14.2 cm/s. ^{24,56} Processes behind filtration include interception, inertial impaction, and diffusion, in addition to electrostatic effects in the case of N95, ^{8,24} and this speed of impact v determines the filtration efficiency. In what follows, we will express the flow rate as well as face velocity, the latter of which permits comparison of filter measurements that used different areas. We emphasize that use of variable size vacuum fittings permits the testing of a

wide range of the face velocities for a given flow range, as shown in Fig. 3(a).

B. Pressure drop over typical filter materials

Breathing through a mask always requires more effort than breathing without one. The resistance to flow of the mask is determined by a combination of filter material and fit and can be quantified by the pressure drop at a given flow. In our experiments, the pressure difference between the SP and SA chambers is the pressure drop over either the mask or material being tested. We measure the pressure drop using a differential pressure gauge (TSI 9565, MN, USA) connected to each chamber by tubing of equal length.

Figure 4(a) shows the pressure drop vs flow for the mannequin head without a mask as well as each of the KF fittings attached to the materials clamp without material inserted. As expected, these constrictions produce a measurable pressure drop much smaller than that of typical masks and materials. Figure 4(b) shows the pressure drop over a set of materials with the KF40 vacuum fitting in the materials clamp. We note, in particular, the large variation of pressure drops among masks labeled N95 and KN95. Large pressure drops across filter material can significantly reduce the protection of a given mask since the required air flow is distributed between the filtered flow through the mask material and the unfiltered leaks around the mask due to an imperfect seal. At a given flow, as the pressure drop across the mask increases, the draw of contaminants through leaks and facial fit gaps increases. We return to this point below in Sec. III D.

C. Filtration efficiency of filter material

Figure 5(a) shows the penetration of all particles >0.3 μ m vs flow rate for certified N95s and many other materials using the KF40 materials tester attachment. The woven bandana material provides very little protection from aerosol in the size range (0.3 μ m-1.0 μ m) of our experiments and yet still has an appreciable pressure drop, which is ~60% of a tested N95. This combination of filtration and pressure drop suggests that efforts to layer the bandana material for more effective filtration could be hindered by breathability limits. Compared to the bandana, the tested surgical mask

has a far superior filtration efficiency of 50% with nearly equivalent breathability, based on its similar pressure drop at the same flow rate. Sterilization wrap has been proposed as a highly efficient filter candidate for improvised PPE approaches⁵⁷ as it is readily available in many clinical settings. Compared to a surgical mask, the material has higher filtration efficiency, but it is less breathable. While offering higher filtration protection, a higher pressure drop means that to sustain a given flow, the pressure across leakages in the facial seal will support more flow, which is detrimental to protection. Another class of potential PPE filter materials is high-efficiency particulate air (HEPA)-type vacuum bags and electrostatic furnace filters with standardized filtration rating systems known as MERV (Minimum Efficiency Reporting Values) and MPR (Microparticle Performance Rating).

The logarithmic scale in Fig. 5(b) brings out the lowpenetration region of interest for the comparison of various highperformance materials. All N95, most KN95, and a polytetrafluoroethylene (PTFE)-coated HEPA filter show >95% filtration efficiency. While the PTFE HEPA material excels at filtration, the pressure drop exceeds the NIOSH breathability limit of 0.343 kPa for inhalation.⁵⁸ Note that one uncertified mask, labeled KN95 No. 3, performs poorly with only ~60% filtration efficiency. While this mask has filtration performance slightly better than a surgical mask, the pressure drop is greater, which means more flow is expected through the small leaks around the mask, and thus, it may not in fact offer more protection in practice. This observation highlights both the importance of local testing of masks and materials that are uncertified or of unclear origin, as well as the need to assess both the filtration and pressure drop properties of materials. While not performed in this study, this analysis would also be well suited for assessing critical changes in material performance due to disinfection and re-use of PPE.

D. Mask facial fit

Sections III B and III C describe tests of pressure drop and filtration efficiency for materials under conditions that should represent a mask perfectly sealed to a user's face. In practice, imperfections of mask fit contribute to varying degrees of total inward

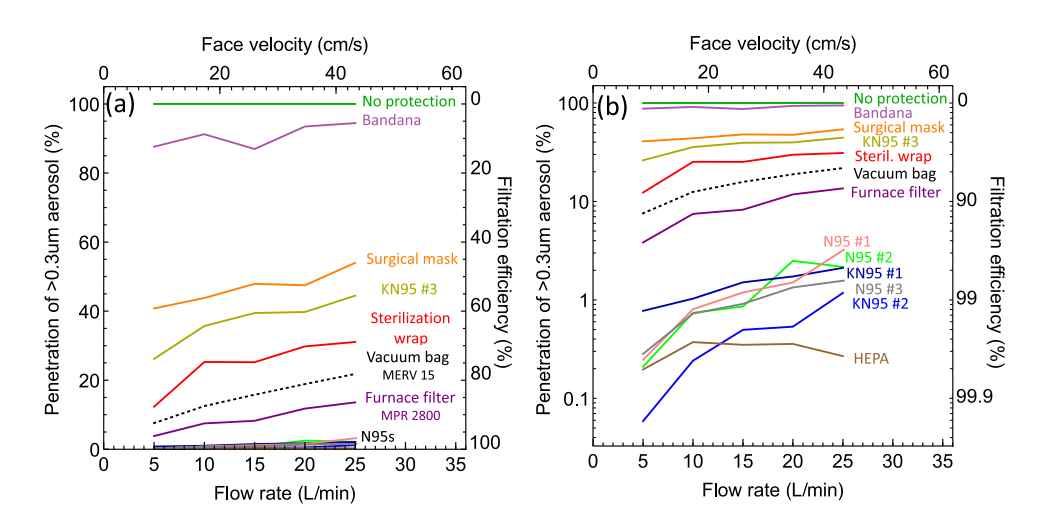


FIG. 5. Relative transmission measurements. (a) Linear and (b) log plot of normalized transmission of select filter materials through the 37 mm ID KF40 flange attachment. Most of the KN95 or N95 mask material we tested complies with the transmission specifications. Alternative filtration media were not close enough to the 5% threshold (gray line) to suggest its widespread use as a replacement to high-grade material.

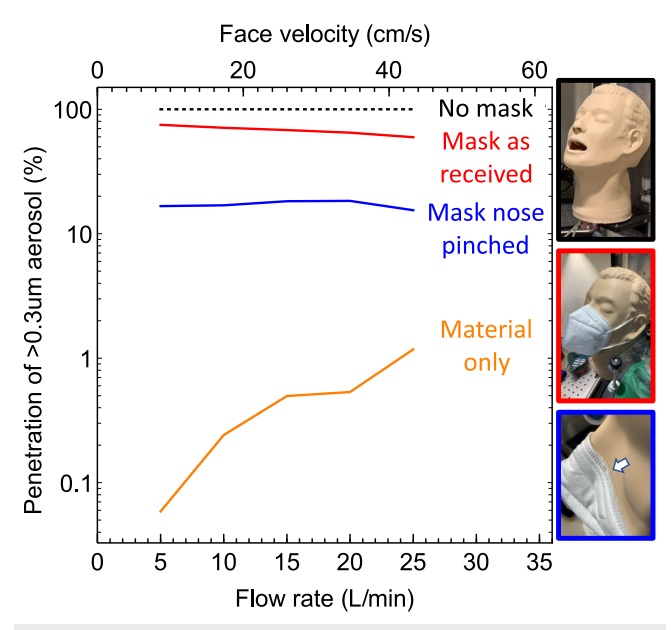


FIG. 6. Mask fit result. A KN95 mask is donned and penetration measured before and after the nose was pinched. These results emphasize the importance of facial fit in effective protection.

leakage.⁵⁹ Inclusion of a second test channel through the mannequin head permits an assessment of mask fit and its potentially deleterious contribution to protection. To expose this sensitivity, Fig. 6 shows the penetration of aerosol through the mannequin head with a mask labeled KN95 before and after attempting to improve the fit by pinching the metal nose piece. The use of a glove box is a necessary feature for making small *in situ* adjustments to study the

facial fit sensitivity. The drastic improvement from >50% penetration to <20% penetration highlights the benefits of tight facial seal. At the same time, the degree of protection is still much less than the material alone, which has a measured penetration of less than 1%. While this system is limited to one facial profile, and established fit testing methods should be applied to any novel mask designs, this exercise demonstrates the ability of the apparatus to rapidly and comprehensively compare the critical elements of mask performance.

IV. CONCLUSIONS

We have demonstrated the construction and evaluation of a fast-turnaround apparatus capable of evaluating three important characteristics of aerosol-filtering masks: breathability quantified through pressure drop, filtration quantified through particulate penetration, and facial fit as determined from direct measurements on a mannequin head form. We have demonstrated the sensitivity of the measurements and considered sources of error in the measurement. We present comparison of high-technology electrostatic filters, surgical masks, instrument wrap fabric, and common textiles against complete lack of protection. The glove box-based design concept has many advantages such as rapid screening of many masks without disrupting aerosol generation and flow. The design can be implemented with resources common to many universities and hospitals and can be implemented with accessible sensors and electronics to screen masks with a range of filtration capabilities.

ACKNOWLEDGMENTS

This work would not be possible without the support of Eleiza Braun, Michael Bailey, Wesley Byerly, Ray Celmer, Jason Chandler,

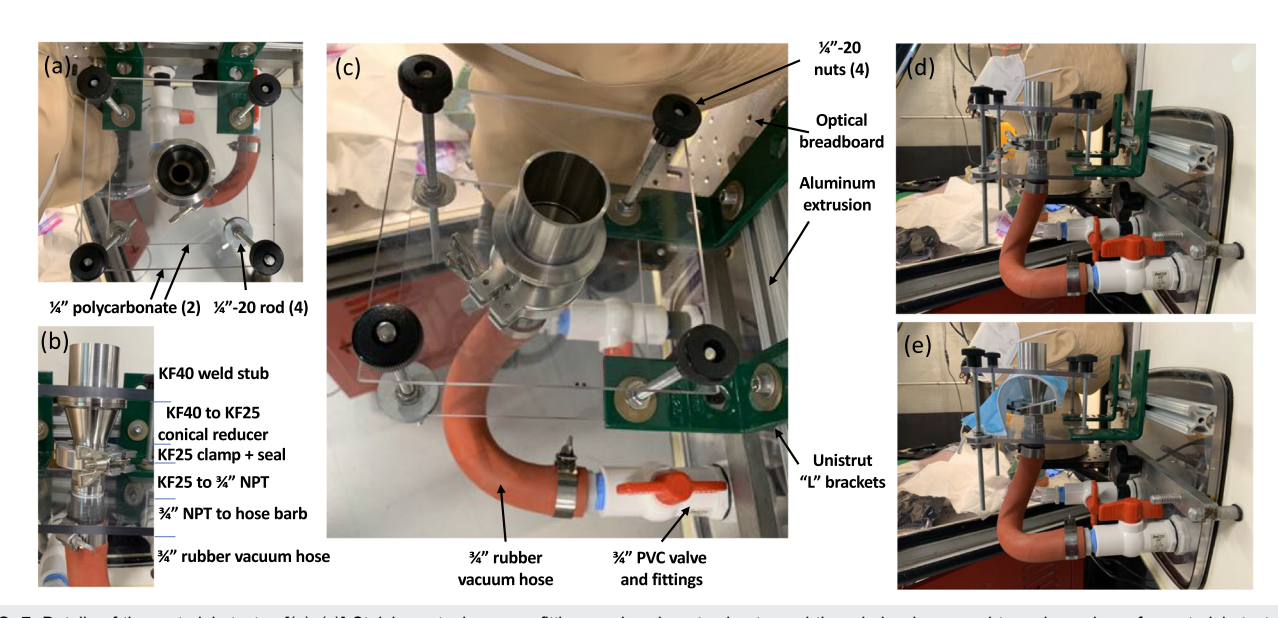
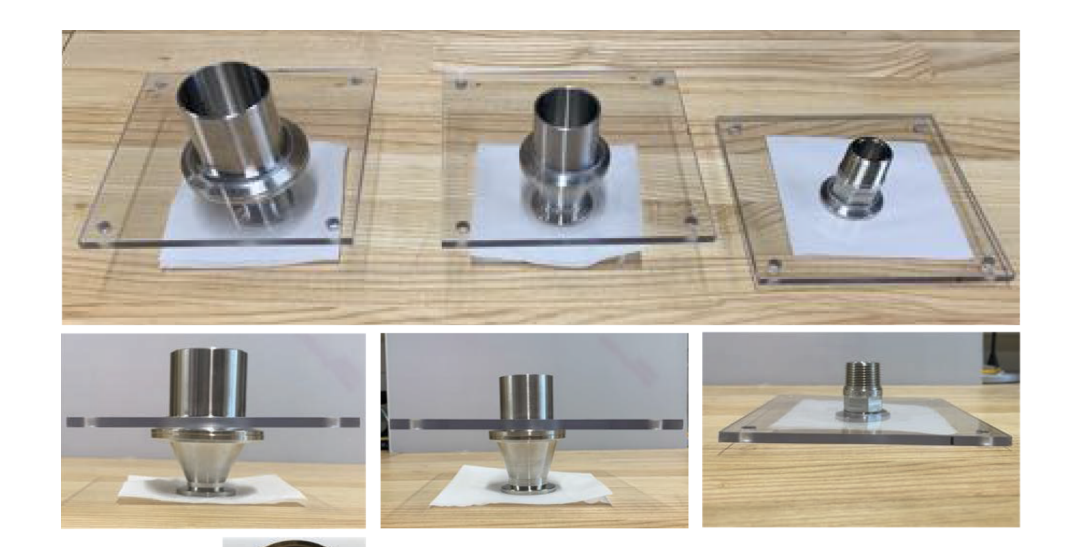


FIG. 7. Details of the materials tester. [(a)–(c)] Stainless steel vacuum fittings, polycarbonate sheets, and threaded rod are used to make a clamp for materials tests. (d) Empty materials tester. (e) Nondestructive testing of a surgical mask.

KF50

47mm ID



KF40

37mm ID

FIG. 8. Three sizes of KF flange permit adjustment of the face velocity for a given flow range.

Tamara Corioso, Terri Dominguez, Mike Jednak, Andrew Kelly, Dave Perry, Cindy Polinksi, and Barrett Wells. The authors would like to thank Livia Daggett, Drew Gentner, Kevin Hsueh, Barbara Mellone, Lisa Lattanza, Shawn London, Michael Plumley, Katherine Schilling, Kristina Wagstrom, Ben Waxman, Whitney Waxman, Larry Wilen, and Christopher Wiles for valuable conversations. They are especially grateful to Adrian Dybwad and PurpleAir for support in designing the software acquisition system. They would also like to thank Joseph Luciani, Matthew Phelps, Amani Jayakody, Asanka Amarasinghe, and Kaitlin Lyszak for assistance and for supporting the work. This work was supported, in part, by National Science Foundation, Grant No. NSF-DMR-1905862.

APPENDIX A: MATERIALS TESTER DETAIL

Figure 7 details the materials tester mechanism. A flow-through clamp is based upon Kwik-Flange vacuum fittings to create a tight and reproducible clamp on thin pieces of material without invasive handling or destruction of the mask or material being tested. The clamp can be operated with the gloves of the glove box, permitting direct comparison of materials with each other or with an empty holder under the same environmental conditions. In order to ensure the mating flanges clamp parallel to one another and form a tight uniform seal on the material, the KF flanges are compressed between two polycarbonate plates using $\frac{1}{4}$ –20 threaded rod as shown. Large knobs on the clamping nuts are convenient for changing masks while using the gloves. An advantage of the KF approach is the possibility to change the filter or mask area being probed, which leads to a change in the tested face velocity range, as illustrated in Fig. 3(a) of the main text. Details of the clamp mechanism options for the three sizes available for the materials tester are shown in Fig. 8.

APPENDIX B: DIRECT FACE VELOCITY MEASUREMENTS

KF25

17.8mm ID

Figure 9 shows the results of an experiment using a hot wire anemometer to directly measure the face velocity across the open weld stub where air enters the materials tester. The lines through the points are the volumetric flow rate divided by the measured area. This plot shows that our face velocities are as expected and that there are no significant leaks in the SP chamber.

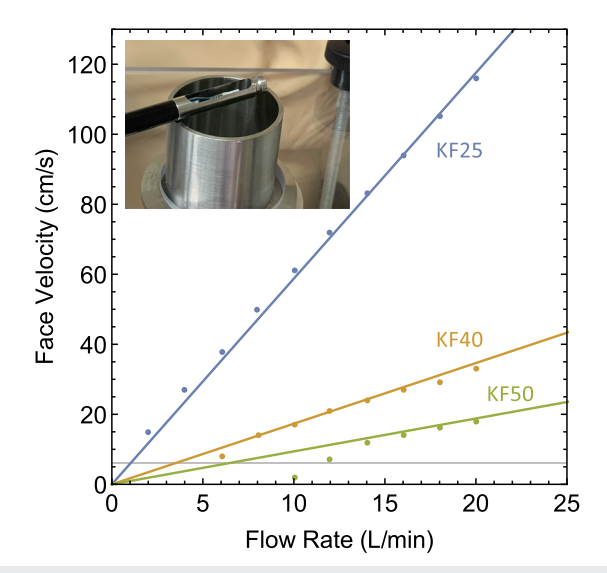


FIG. 9. Results of the anemometer face velocity measurement (points) along with the volumetric flow divided by the KF weld stub inner area (lines).

DATA AVAILABILITY

The data that support the findings of this study are available from the corresponding author upon reasonable request.

REFERENCES

- ¹Y. Liu, Z. Ning, Y. Chen, M. Guo, Y. Liu, N. K. Gali, L. Sun, Y. Duan, J. Cai, D. Westerdahl, X. Liu, K. Xu, K.-f. Ho, H. Kan, Q. Fu, and K. Lan, "Aerodynamic analysis of SARS-CoV-2 in two Wuhan hospitals," Nature **582**, 557 (2020).
- ²WHO, Modes of transmission of virus causing COVID-19: Implications for IPC precaution recommendations, World Health Organization Scientific Brief, 2020.
- ³ National Academies of Sciences, Engineering, and Medicine, *Rapid Expert Consultation on the Possibility of Bioaerosol Spread of SARS-CoV-2 for the COVID-19 Pandemic* (The National Academies Press, Washington, DC, 2020).
- ⁴L. Morawska and J. Cao, "Airborne transmission of SARS-CoV-2: The world should face the reality," Environ. Int. **139**, 105730 (2020).
- ⁵CDC, Interim infection prevention and control recommendations for patients with suspected or confirmed coronavirus disease 2019 (COVID-19) in healthcare settings, Center for Disease Control, 2020.
- ⁶CDC, Healthcare infection prevention and control FAQs for COVID-19, 2020.
- $^{7}\rm{G}$. Kates, "N95 mask shortage comes down to this key material: 'The supply chain has gotten nuts'," CBS News, 2020.
- ⁸P. D. Tsai, "Information and FAQs—Charged filtration material performance after various sterilization techniques," University of Tennessee Research Foundation, 2020.
- ⁹O. Khazan, Why We're Running Out of Masks (The Atlantic, 2020).
- ¹⁰P. J. Kapust, Osha enforcement guidance for respiratory protection and the N95 shortage due to the coronavirus disease 2019 (COVID-19) pandemic, 2020.
- ¹¹P. Wehner, NIH Director: 'We're on An Exponential Curve' (The Atlantic, 2020).
- ¹²J. Whalen, Change in U.S. law will make millions more masks available to doctors and nurses, white house says, Washington Post, 2020.
- ¹³ N. Lamont, State of Connecticut, executive order No. 7BB.: Protection of public health and safety during COVID-10 pandemic and response—Use of facemasks or cloth face coverings, rescheduling of presidential preference primary to August 11, 2020.
- $^{14}\mathrm{C}.$ Dall, As pandemic rages, PPE supply remains a problem, CIDRAP, 2020.
- ¹⁵ A. Hufford, "N95 face mask makers ramp up production to meet U.S. COVID-19 demand," Wall St. J. (2020), available at https://www.wsj.com/articles/n95-mask-makers-ramp-up-production-to-meet-u-s-covid-19-demand-11594987201.
- ¹⁶ A. Konda, A. Prakash, G. A. Moss, M. Schmoldt, G. D. Grant, and S. Guha, "Aerosol filtration efficiency of common fabrics used in respiratory cloth masks," ACS Nano 14, 6339 (2020).
- ¹⁷CDC, Use of cloth face coverings to help slow the spread of COVID-19, Center for Disease Control, 2020.
- 18 J. Bort, Using blue shop towels in homemade face masks can filter particles $2\times$ to $3\times$ better than cotton, 3 clothing designers discover after testing dozens of fabrics, Business Insider, 2020.
- ¹⁹ J. D. Noti, W. G. Lindsley, F. M. Blachere, G. Cao, M. L. Kashon, R. E. Thewlis, C. M. McMillen, W. P. King, J. V. Szalajda, and D. H. Beezhold, "Detection of infectious influenza virus in cough aerosols generated in a simulated patient examination room," Clin. Infect. Dis. 54, 1569–1577 (2012).
- ²⁰T. Jefferson, M. Jones, L. A. Al Ansari, G. Bawazeer, E. Beller, J. Clark, J. Conly, C. Del Mar, E. Dooley, E. Ferroni, P. Glasziou, T. Hoffman, S. Thorning, and M. Van Driel, "Physical interventions to interrupt or reduce the spread of respiratory viruses. Part 1. Face masks, eye protection and person distancing: Systematic review and meta-analysis," medRxiv:10.1101/2020.03.30.20047217.
- ²¹ J. D. Smith, C. C. MacDougall, J. Johnstone, R. A. Copes, B. Schwartz, and G. E. Garber, "Effectiveness of N95 respirators versus surgical masks in protecting health care workers from acute respiratory infection: A systematic review and meta-analysis," Can. Med. Assoc. J. 188, 567–574 (2016).
- ²²M. Loeb, N. Dafoe, J. Mahony, M. John, A. Sarabia, V. Glavin, R. Webby, M. Smieja, D. J. D. Earn, S. Chong, A. Webb, and S. D. Walter, "Surgical mask vs N95 respirator for preventing influenza among health care workers: A randomized trial," J. Am. Med. Assoc. 302, 1865–1871 (2009).

- ²³ N. H. L. Leung, D. K. W. Chu, E. Y. C. Shiu, K.-H. Chan, J. J. McDevitt, B. J. P. Hau, H.-L. Yen, Y. Li, D. K. M. Ip, J. S. M. Peiris, W.-H. Seto, G. M. Leung, D. K. Milton, and B. J. Cowling, "Respiratory virus shedding in exhaled breath and efficacy of face masks," Nat. Med. 26, 676–680 (2020).
- 24 S. Rengasamy, R. Shaffer, B. Williams, and S. Smit, "A comparison of facemask and respirator filtration test methods," J. Occup. Environ. Hyg. 14, 92–103 (2017).
 25 L. M. Brosseau and M. Sietsema, Masks-for-all for COVID-19 not based on sound data, CIDRAP, 2020.
- ²⁶ K. Schilling, D. R. Gentner, L. Wilen, A. Medina, C. Buehler, K. J. G. Pollitt, R. Bergemann, N. Bernardo, J. Peccia, V. Wilczynski, and L. Lattanza, "An accessible method for screening aerosol filtration identifies poor-performing commercial masks and respirators," J. Exposure Sci. Environ. Epidemiol. (published online) (2020).
- ²⁷ M. Zhao, L. Liao, W. Xiao, X. Yu, H. Wang, Q. Wang, Y. L. Lin, F. S. Kilinc-Balci, A. Price, L. Chu, M. C. Chu, S. Chu, and Y. Cui, "Household materials selection for homemade cloth face coverings and their filtration efficiency enhancement with triboelectric charging," Nano Lett. 20, 5544–5552 (2020).
- ²⁸C. D. Zangmeister, J. G. Radney, E. P. Vicenzi, and J. L. Weaver, "Filtration efficiencies of nanoscale aerosol by cloth mask materials used to slow the spread of SARS-CoV-2," ACS Nano 14, 9188–9200 (2020).
- $^{\mathbf{29}}$ WHO, Advice on the use of masks in the context of COVID-19: Interim guidance, 5 June 2020; accessed on 6 June 2020.
- ³⁰Q. Ou, C. Pei, S. Chan Kim, E. Abell, and D. Y. H. Pui, "Evaluation of decontamination methods for commercial and alternative respirator and mask materials-view from filtration aspect," J. Aerosol Sci. 150, 105609 (2020).
- ³¹ L. Anderegg, C. Meisenhelder, C. O. Ngooi, L. Liao, W. Xiao, S. Chu, Y. Cui, and J. M. Doyle, "A scalable method of applying heat and humidity for decontamination of N95 respirators during the COVID-19 crisis," PLOS One (published online) (2020).
- ³²K. Rogers, "All your questions about how to wear a face mask—Answered," CNN, April 24, 2020.
- ³³ M. Cascella, M. Rajnik, A. Cuomo, S. C. Dulebohn, and R. Di Napoli, *Features, Evaluation and Treatment Coronavirus (COVID-19)* (StatPearls Publishing, Treasure Island, FL, 2020).
- ³⁴E. P. Vejerano and L. C. Marr, "Physico-chemical characteristics of evaporating respiratory fluid droplets," J. R. Soc., Interface. 15, 20170939 (2018).
- ³⁵W. Wells, Airborne Contagion and Air Hygiene: An Ecological Study of Droplet Infections (Commonwealth Fund, 1955).
- ³⁶X. Xie, Y. Li, A. T. Y. Chwang, P. L. Ho, and W. H. Seto, "How far droplets can move in indoor environments–revisiting the wells evaporation-falling curve," Indoor Air 17, 211–225 (2007).
- ³⁷J. Atkinson, Y. Chartier, C. L. Pessoa-Silva, P. Jensen, Y. Li, and W.-H. Seto, "Natural ventilation for infection control in health-care settings," World Health Organization, 2020.
- ³⁸Y. M. Bar-On, A. Flamholz, R. Phillips, and R. Milo, "SARS-CoV-2 (COVID-19) by the numbers," eLife Sci. Publ. **9**, e57309 (2020).
- ³⁹ N. van Doremalen, T. Bushmaker, D. H. Morris, M. G. Holbrook, A. Gamble, B. N. Williamson, A. Tamin, J. L. Harcourt, N. J. Thornburg, S. I. Gerber, J. O. Lloyd-Smith, E. de Wit, and V. J. Munster, "Aerosol and surface stability of SARS-CoV-2 as compared with SARS-CoV-1," N. Engl. J. Med. 382, 1564–1567 (2020).
- ⁴⁰E. Y. C. Shiu, N. H. L. Leung, and B. J. Cowling, "Controversy around airborne versus droplet transmission of respiratory viruses: Implication for infection prevention," Curr. Opin. Infect. Dis. 32(4), 372 (2019).
- ⁴¹R. Tellier, Y. Li, B. J. Cowling, and J. W. Tang, "Recognition of aerosol transmission of infectious agents: A commentary," BMC Infect. Dis. **19**, 101 (2010)
- ⁴²S. Kooij, A. Astefanei, G. L. Corthals, and D. Bonn, "Size distributions of droplets produced by ultrasonic nebulizers," Sci. Rep. 9, 6128 (2019).
- ⁴³Nelson Labs, Particle filtration efficiency test, 2020.
- ⁴⁴NIOSH, Determination of particulate filter efficiency level for N95 series filters against solid particulates for non-powered, air purifying respirators standard test procedure, CDC, 2019.
- ⁴⁵M. Echols and J. A. Young, Studies of Portable Air-Operated Aerosol Generator (U.S. Naval Research Laboratory, Washington, DC, 1963).

- ⁴⁶W. C. Hinds, J. M. Macher, and M. W. First, "Size distribution of aerosols produced by the Laskin aerosol generator using substitute materials for DOP," Am. Ind. Hyg. Assoc. J. **44**, 495–500 (1983).
- ⁴⁷J. Smolik, L. Dzumbova, J. Schwarz, and M. Kulmala, "Evaporation of ventilated water droplet: Connection between heat and mass transfer," J. Aerosol Sci. 32, 739–748 (2001).
- ⁴⁸W. C. Hinds, Aerosol Technology: Properties, Behavior, and Measurement of Airborne Particles (Wiley & Sons, Inc., 1999).
- ⁴⁹ ASTM, F2299-03, standard test method for determining the initial efficiency of materials used in medical face masks to penetration by particulates using latex spheres, 2003.
- ⁵⁰ ASTM, Standard specification for performance of materials used in medical face masks, 2019.
- ⁵¹M. Levy Zamora, F. Xiong, D. Gentner, B. Kerkez, J. Kohrman-Glaser, and K. Koehler, "Field and laboratory evaluations of the low-cost plan tower particulate matter sensor," Environ. Sci. Technol. **53**, 838–849 (2019).
- ⁵² M. Bergman, Z. Zhuang, and R. E. Shaffer, Advanced headforms for evaluating respirator fit, CDC, 2013.
- ⁵³P. Kumar, P. Fennell, J. Symonds, and R. Britter, "Treatment of losses of ultrafine aerosol particles in long sampling tubes during ambient measurements," Atmos. Environ. 42, 8819–8826 (2008).
- ⁵⁴C. Chourpiliadis and A. Bhardwaj, *Physiology, Respiratory Rate* (StatPearls, 2020).

- 55 FDA, Guidance for industry and FDA staff surgical masks, FDA, 2004.
- ⁵⁶S. Rengasamy, A. Miller, B. Eimer, and R. Shaffer, "Filtration performance of FDA-cleared surgical masks," J. Int. Soc. Respir. Prot. 26, 54–70 (2009).
- $^{\bf 57}{\rm E.}$ Thompson, UF doctor invents new type of mask to help offset coronavirus shortage, Orlando Sentinel, 2020.
- ⁵⁸L. Rosenstock, "42 CFR part 84: Respiratory protective devices implications for tuberculosis protection," Infect. Control Hosp. Epidemiol. **16**, 529–531 (1995).
- ⁵⁹S. Rengasamy, B. C. Eimer, and J. Szalajda, "A quantitative assessment of the total inward leakage of NaCl aerosol representing submicron-size bioaerosol through N95 filtering facepiece respirators and surgical masks," J. Occup. Environ. Hyg. 11, 388–396 (2014).
- ⁶⁰ J. N. Hancock, M. J. Plumley, K. Schilling, D. Sheets, and L. Wilen, ACS Nano. 14(9), 10758–10763 (2020).
- ⁶¹ A. Rule, G. Ramachandran, and K. Koehler, ACS Nano. **14**(9), 10756–10757 (2020)
- ⁶²I. A. Carr, P. Hariharan, and S. Guha, ACS Nano. **14**(9), 10754–10755 (2020).
- ⁶³ A. Konda, A. Prakash, G. A. Moss, M. Schmoldt, G. D. Grant, and S. Guha, ACS Nano. 14(9), 10764–10770 (2020).
- ⁶⁴ A. Konda, A. Prakash, G. Moss, M. Schmoldt, G. Grant, and S. Guha, ACS Nano. 14(8), 10742–10743 (2020).